

Missing Rung Problem in Vibrational Ladder Climbing

Takahiro Horiba, Soichi Shirai, and Hirotooshi Hirai*

*Toyota Central Research and Development Labs., Inc.,
41-1, Yokomichi, Nagakute, Aichi 480-1192, Japan*

(Dated: October 23, 2021)

We discovered the vanishment of the transition dipole moment that interrupts the vibrational ladder climbing (VLC) in molecular system. We clarified the mechanism of that and present the method utilizing the additional chirped pulse to keep the VLC. To show the power of our method, we conducted the wavepacket dynamics simulations for LiH dissociations with chirped pulses. The result indicates that the efficiency of LiH dissociation is significantly improved by our method compared to conventional methods. We also revealed the quantum interference effect behind the excitation process of VLC.

Controlling molecular reactions as desired is one of the ultimate goals of chemistry. Unlike the conventional macroscopic reaction control methods using temperature and pressure, methods that directly control the quantum state of molecules using the electric field of a laser has been proposed to dramatically improve the efficiency and selectivity of reactions [1–3]. This kind of techniques, which originated in Brumer and Shapiro’s proposal in the 1980s[1], is called “coherent control”, and with the birth of femtosecond pulsed lasers and the development of laser shaping technology, it has been the subject of numerous studies and continues to attract a great deal of attention[4–6]. One of the promising method in such techniques is the Vibrational Ladder Climbing (VLC)[7]. That is the cascade excitation process in molecular vibrational levels under chirped infrared laser pulses whose time-dependent frequency corresponds to each vibrational excitation energy. The VLC can focus the input laser pulse energy on a specific molecular bond. Thereby, it is expected to realize highly efficient bond-selective photodissociation[8]. From the both experimental and theoretical aspects, the VLC has been studied intensively. In experimental researches, the vibrational excitation by the VLC in diatomic molecules (NO[9], HF[10]) and amino acids[11] etc. have been reported. Recently, Morichika et al. succeeded in breaking molecular bonds in transition metal carbonyl WCO_6 with the chirped infrared pulse enhanced by the surface plasmon resonance[8]. Unfortunately, there are few experimental reports on such a successes of bond breaking by the VLC, which is still a challenging issue at present. In early theoretical works done by Liu and Yuan et al., the classical motion of driven Morse oscillators were studied[12–14]. They analyzed the excitation and dissociation dynamics of diatomic molecules under a chirped electric field using the action-angle variable, and found the condition for the efficient excitation[12, 13]. While in the quantum aspects, a pioneering work was done by Friedland et al[15]. They focused on quantum and classical excitation process; the quantum ladder climbing and the classical autoresonance, and proposed the parameters, that characterize quantum and classical

phenomena[15, 16]. Based on the characterization parameters, quantum and classical comparisons were made in various systems[17–20] such as plasma systems[21] and superconducting circuits[22]. The excitation condition proposed by Yuan et al. and the characterization parameters proposed by Friedland et al. depend on the physical properties of the system such as the potential energy surface (PES) and the dipole function. Thereby, those properties determine the characteristic of the VLC. Most of theoretical researches were, however, based on simple model functions of them such as Morse potentials and the linear dipole moments[12, 15, 23–25].

In this study, we performed wavepacket dynamics simulations of the VLC based on the PES and the dipole moment computed by highly accurate *ab-initio* quantum chemistry method. The results of the simulations revealed the problem that has not been recognized in the VLC: the VLC is interrupted because of the existence of the level which has nearly zero adjacent transition dipole moment (TDM), i.e. the vanishment of TDMs. We call this problem “Missing Rung Problem” (MRP) as it’s like the rung is missing in the middle of ladder. To clarify the issue in more detail, the PESs and the TDMs of the diatomic molecules LiH and HF are shown in Fig. 1(b) and (c), respectively. It can be seen that the TDMs of the 16th level of LiH and the 12th levels of HF, have nearly zero values, which indicate the “Missing Rung” in vibrational levels.

In order to understand the cause of MRP, we will start the discussion by considering a harmonic oscillator. The vibrational wave functions of the harmonic potential $|\phi_i\rangle$ are described by Hermite polynomial, and their parities are different from those of adjacent levels as described in Fig. 1(a). Assuming odd function as a dipole moment, TDMs between adjacent levels $\mu_{i,i+1} = \langle \phi_i | \mu | \phi_{i+1} \rangle$ become an integral of even function, which yields the nonzero value (i.e. allowed transition). The well-known infrared selection rule (i.e. $\Delta\nu = \pm 1$) corresponds to this result[26]. On the other hand, if we assume the even function as the dipole moment, the adjacent TDM $\mu_{i,i+1}$ become an integral of odd function, which yields zero (i.e. forbidden transition) as shown in

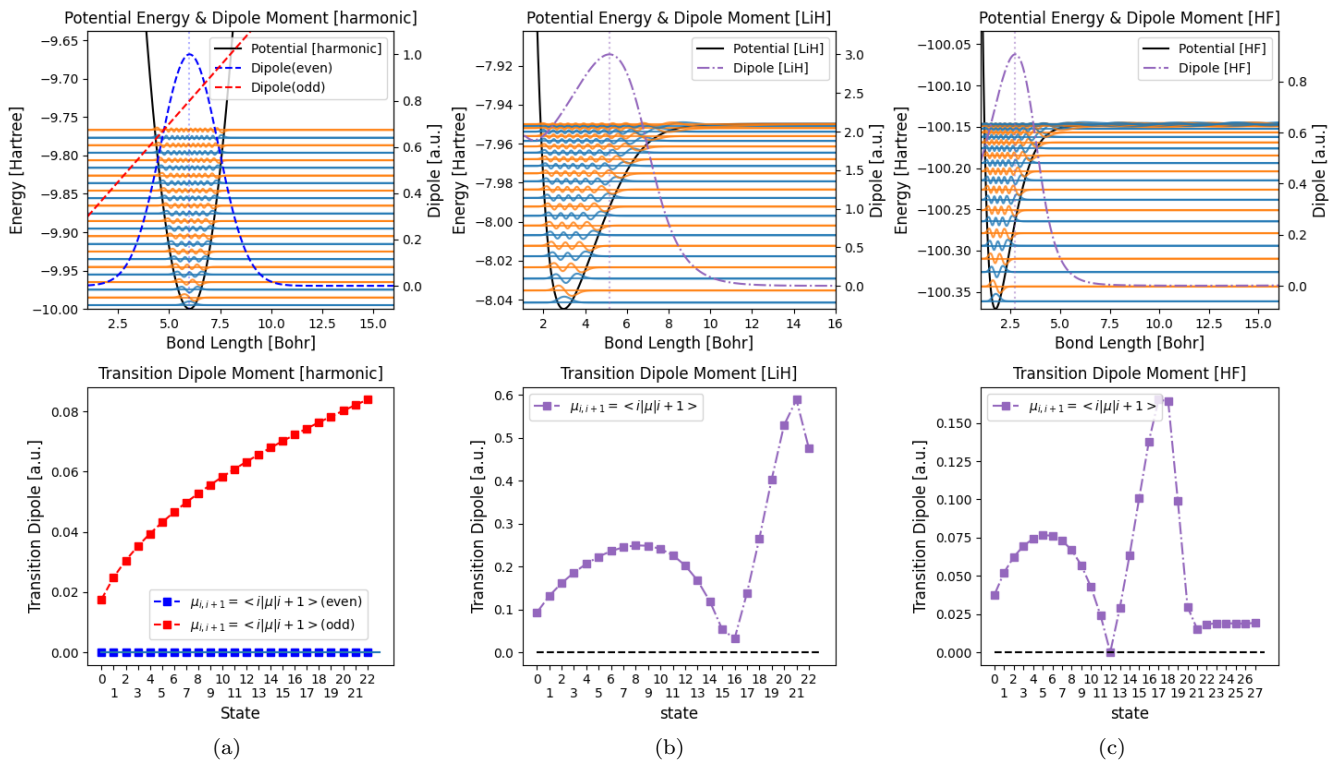


FIG. 1: Upper panels: The PESs and the dipole moments for (a) the harmonic model, (b) LiH molecule and (c) HF molecule. In the harmonic model, the model dipole moments are shown. Lower panels: the corresponding TDMs.

the lower panel of Fig. 1(a).

Based on the above discussions, we consider realistic molecular systems. The shape of vibrational wave functions of molecules are similar to that of the harmonic potential (see Figs. 1(b) LiH and (c) HF) except the distortion due to the anharmonicity of the PESs. Therefore, the nature of parity of wave functions is approximately conserved. Whereas the parity of molecular dipole moments is not as simple as the above discussions. Near the equilibrium distance, the dipole moment can be regarded as linear (i.e. odd function-like). Thereby, the TDM $\mu_{i,i+1}$ increases monotonically as the vibrational level becomes higher like the harmonic model. As the bond length increases, however, the nonlinearity of the dipole moment appears. The dipole function takes maxima (i.e. even function-like) and then asymptotes to zero. This behavior results from the relaxation of the molecular polarization, which is ubiquitous for charge neutral heteronuclear diatomic molecules. As the edge of the distribution of the i th vibrational level of the wavefunction reaches to the maxima point of the dipole function, the TDM $\mu_{i,i+1}$ begins to decrease due to the even-function nature of the dipole function. Then the TDM has the near zero value as can be seen in Fig.1(b) and (c) for the case of LiH and HF, respectively. The "Missing Rung" will not appear in the VLC simulations based on the as-

sumption of the linear dipole function and will be likely to give unrealistic result. Since the position of "Missing Rung" is sensitively depends on the shape of the PES and dipole function (see Supplemental materials), it is necessary to perform highly-accurate quantum chemistry methods to identify its exact position.

In order to verify the existence of the "Missing Rung" definitely by the numerical experiments, we conducted wavepacket dynamics simulations for LiH molecule. The time evolution of the wavepacket $\Psi(x, t)$ under the laser electric field $E(t)$ is expressed by the following time-dependent Schrödinger equation

$$i\hbar \frac{\partial}{\partial t} \Psi(x, t) = H(x, t) \Psi(x, t), \quad (1)$$

where the Hamiltonian $H(x, t)$ is defined by

$$H(x, t) = H_0(x) - \mu(x)E(t) \quad (2)$$

$$H_0(x) = -\frac{\hbar^2}{2M_{\text{red}}} \frac{\partial^2}{\partial x^2} + V(x). \quad (3)$$

M_{red} in the $H_0(x)$ is the reduced mass of LiH. The potential energy $V(x)$ and the dipole moment $\mu(x)$ were calculated by multireference averaged quadratic coupled-cluster(MR-AQCC) method[27]. Details of these computations are described in supplemental materials. We employ the Gaussian pulse as the electric field $E(t)$ of the

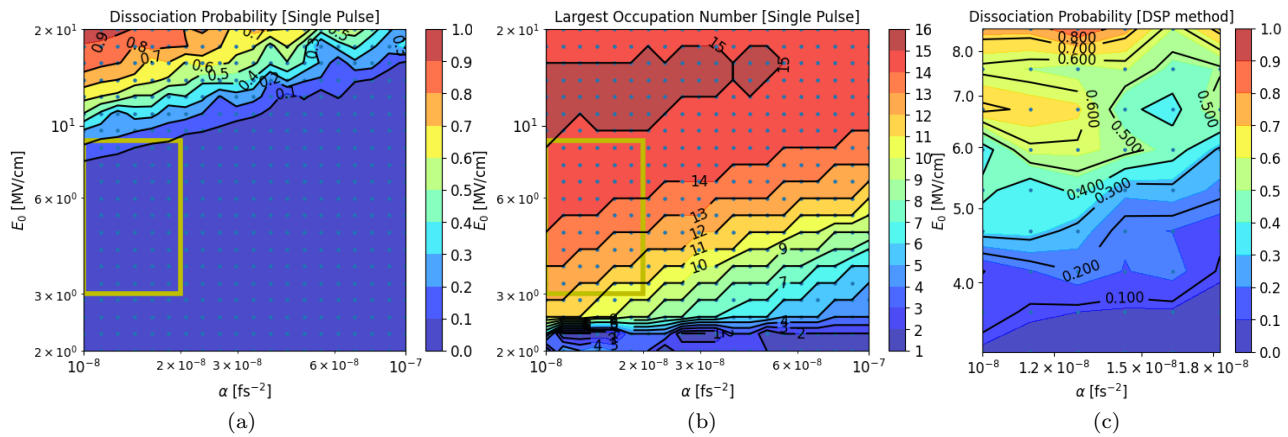


FIG. 2: The color maps of the results of the single pulse method and the DSP method (explained later in this paper). (a)Dissociation probabilities and (b)the vibrational state that has the largest occupation number for the single pulse method. (c)Dissociation probabilities for the DSP method. Blue dots represent the grid points where the wavepacket simulations were conducted. Yellow boxed area in (a)(b) represents the parameter range chosen for the DSP method.

pulsed laser. The formula of $E(t)$ is determined as the following,

$$E(t) = E_0 \exp^{-\alpha(t-t_0)^2} \cos \omega(t)(t-t_0), \quad (4)$$

where E_0 is the maximum electric field intensity, α is the spreading parameter of the Gaussian, t_0 is the center time of the pulse, and $\omega(t)$ is the time-dependent frequency. The time variation of $\omega(t)$ is assumed to be linear chirp, and parametrized by the two dimensionless parameters γ_1 and γ_2 as follows,

$$\omega(t) = \omega_0 \left\{ -(\gamma_1 + \gamma_2) \cdot \frac{t-t_0}{4\sigma} + 1 + \frac{\gamma_1 - \gamma_2}{2} \right\}, \quad (5)$$

where $\sigma = 1/\sqrt{2\alpha}$ is the standard deviation of the Gaussian pulse envelope. Equation 5 means that $\omega(t)$ is a linear function through two points, $\omega(t_0 - 2\sigma) = \omega_0(1 + \gamma_1)$ and $\omega(t_0 + 2\sigma) = \omega_0(1 - \gamma_2)$. The reference frequency ω_0 was set to the transition frequency between the grand state and the first excited state ($\omega_0 = (E_1 - E_0)/\hbar$). Based on the above formulation, the VLC process of LiH molecule was simulated by computing the time evolution of wavepackets that initially set to the ground state using the second-order Suzuki-Trotter decomposition method. Here, we discuss the parameter ranges of E_0 and α that determine the shape of pulses. As mentioned in the introduction, there are two types of mechanisms of excitation process induced by chirped lasers: quantum ladder climbing and classical autoresonance. Since MRP is a quantum issue that apparently appears when the vibrational levels can be regarded as discrete, the parameter range should be chosen as quantum ladder climbing occurs. Therefore, using the characterization parameters proposed by Friedland et al[16], we estimated the parameter range that can be classified to quantum ladder

climbing (see supplementary materials for details). As the result, the parameter range was determined to be $E_0 = 2.0 - 20$ [MV/cm], $\alpha = 10^{-8} - 10^{-7}$ [fs $^{-2}$]. For this parameter range of E_0 and α , 20×20 grid points on logarithmic scales is obtained. The wavepacket dynamics simulations were carried out for the each grid point. The chirp parameters γ_1, γ_2 were optimized by the Bayesian optimization so as to maximize the degree of the excitation and the dissociation probability. The degree of excitation is evaluated by the expectation value of the occupied states, and the dissociation probability is evaluated by time-integration of the probability density flux of the wavepacket that reaches the dissociation limit. The details of the wavepacket simulations and optimizations are described in supplementary material.

Figure 2(a) and (b) shows the results of the wavepacket dynamics simulations with optimized chirp parameters. The color map in Fig. 2(a) shows the dissociation probabilities, showing the trend that the dissociation probabilities get larger with larger electric fields ($\propto E_0$) and longer pulse widths ($\propto 1/\sqrt{\alpha}$). This result is the natural consequence of the fact that the more dissociation is promoted with the higher pulse energy. The color map in Fig. 2(b) shows the vibrational state that has the largest occupation number (excluding the ground state) after each of the simulations. It can be seen that there is a wide plateau consisting of the 15th and 16th states. Since the ‘‘Missing Rung’’ of LiH is located around the 16th state, this result indicates that the wavepacket was trapped there due to the ‘‘Missing Rung’’ during the VLC. As shown in the above result, the MRP hinder the photodissociation by VLC. Since the MRP is the ubiquitous problem for molecular bonds with polarization, it is significantly important to solve the MRP in order to achieve

the photodissociation by VLC.

Here, we propose the Double-Stepping Pulse (DSP) method as a solution for the MRP. In addition to a conventional pulse for the adjacent transitions ($\Delta\nu = \pm 1$), the DSP method uses the secondary pulse to achieve transitions of $\Delta\nu = \pm 2$, i.e. double stepping, between levels around the ‘‘Missing Rung’’. Based on the previous discussion, when the dipole function has an even function property around ‘‘Missing Rung’’, transitions between the levels of the different parity ($\Delta\nu = \pm 1$) are forbidden, while transitions between the levels of the same parity ($\Delta\nu = \pm 2$) are allowed. And vice versa when the dipole function has an odd function property (see supplementary material). Thereby, the DSP is complementary to a conventional pulse for the successful VLC.

To show the power of our method, we conducted the wavepacket dynamics simulations of the DSP method. We choose the pulse parameters ($E_0 = 3.0 - 9.0$ [MV/cm], $\alpha = 1.0 \times 10^{-8} - 2.0 \times 10^{-8}$ [fs $^{-2}$]: 9×6 grid points on logarithmic scales, as shown in the yellow boxed area in Figs. 2), where almost no dissociation occurred using the single pulse, and adopted them as the main pulse for the transitions of $\Delta\nu = \pm 1$. For the DSP, the pulse parameters, $E_0 = 3.0$ [MV/cm], $\alpha = 8.0 \times 10^{-8}$ [fs $^{-2}$] were used. Here, we have to optimize the chirp parameters for two pulses; the main pulse and the DSP and the delay time between the two pulses ($\Delta t_0 = t_0^{\text{main}} - t_0^{\text{DSP}}$). Thereby, the number of parameters to be optimized is five; $\gamma_1^{\text{main}}, \gamma_2^{\text{main}}, \gamma_1^{\text{DSP}}, \gamma_2^{\text{DSP}}$ and Δt_0 . Since five variables are difficult to handle in Bayesian optimization in terms of computational cost, the CMA-ES[28], that is one of the evolutionary optimization methods, was used for the parameter optimization (see supplementary material for details). The reference frequency of the DSP is set to the transition frequency between 15th \rightarrow 17th levels ($\omega_0^{\text{DSP}} = (E_{17} - E_{15})/\hbar$), where most of the wavepackets were trapped as shown in 2(b). The relative phase between the main pulse and the DSP was set to zero.

The dissociation probabilities obtained by the DSP method are shown in Fig.2(c). It can be seen that the DSP method enhances the dissociation significantly compared to the single pulse method (Fig.2(a)). Although this result shows the superiority of the DSP method over the single-pulse method in terms of the dissociation probabilities, there is the concern about the energy efficiency for the DSP method because the method requires the additional energy to generate the additional pulse. Thus we compared the energy efficiency (the amount of the dissociated molecules per the energy of pulses) for the two methods (Details of the calculation method are described in Supplementary Material). The highest energy efficiency value for the DSP method was 0.763 [mol/J]. On the other hand, that for the single pulse method was 0.193 [mol/J]. Thus, the DSP method was found to be about four times more efficient than the single pulse method, indicating the DSP method is the promising

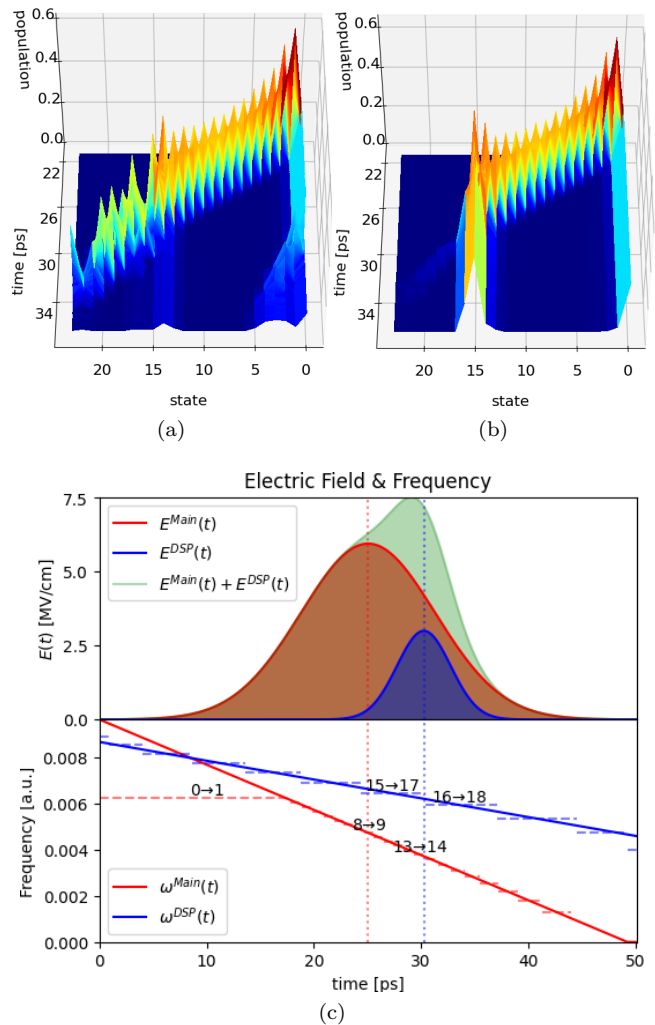


FIG. 3: (a) Snapshot of the excitation process with the most energy efficient pulses in the DSP method. The pulse parameters of the main pulse are $E_0 = 5.95$ [MV/cm], $\alpha = 1.27 \times 10^{-8}$ [fs $^{-2}$]. (b) Snapshot of the excitation process with only the main pulse used in the case of (a). (c) Upper panel: The electric field intensities of the main pulse, the DSP, and the overall field. Lower panel: The corresponding time-dependent frequencies of the main pulse and the DSP in (a).

method as a solution of MRP.

Figure 3(a) shows the snapshot of the wavepacket dynamics simulations with the most energy efficient pulses in the DSP method. Figure 3(b) shows the snapshot with only the main pulse in Fig. 3(b). Without the DSP (Fig 3(b)), it is clearly seen that the wavepacket is trapped in the ‘‘Missing Rung’’ level, while with DSP (Fig 3(a)), the wavepacket is successfully excited to the dissociation limit. Figure 3(c) shows the electric fields and time-dependent frequencies used for the above simulation shown in Fig 3(a). It clearly shows that the DSP is fo-

cused on the 15th and 16th excitation frequencies which are around “Missing Rung”.

However, the above discussions were limited to phenomenological ones. To understand the mechanism of the DSP method in microscopic way, we propose the analysis method that clarifies the dynamics of the vibrational levels under electric fields. Under the arbitrary electric field $E(t)$, the time evolution of the probability amplitude c_j of the j th level, is expressed by the following equation,

$$i\hbar \frac{\partial c_j}{\partial t} = \epsilon_j c_j - \sum_{k \neq j} \mu_{j,k} E(t) c_k, \quad (6)$$

where ϵ_j is the eigenenergy of j th level and $\mu_{j,k}$ is the TDM of j th and k th level. Approximately, the variation of the probability amplitude Δc_j during Δt can be written as,

$$\Delta c_j \simeq -i \frac{\epsilon_j \Delta t}{\hbar} c_j + i \frac{\Delta t}{\hbar} \sum_{k \neq j} \mu_{j,k} E(t) c_k. \quad (7)$$

Figure 4(a) illustrates the meaning of the Eq.7. The first term of the right hand side of the Eq. 7 does not change the norm of c_j since it merely rotates c_j in the complex plane. On the other hand, the second term, which cause the mixing with other levels via the electric field, affects the norm of c_j . As shown in Fig 4(a), it is the radial component of the second term that changes the norm of c_j . Therefore, the contribution to the norm of c_j can be quantified through rotating Δc_j by the argument of c_j : $\theta_j = \arg c_j$ and taking its real part. The summation of the second term represents the contributions to c_j from each level. We define $\Delta C_j^{(k)}(t)$ as the time integration of the contribution to the j th level from the k th level,

indicating the net contribution of the k th level to the j th level norm up to time t . It is written as,

$$\Delta C_j^{(k)}(t) = \int_{-\infty}^t \text{Re} \left(i \frac{\mu_{j,k} E(t')}{\hbar} c_k(t') \exp(-i\theta_j(t')) \right) dt'. \quad (8)$$

A positive value of Eq. 8 means that the k th level acts to increase the norm of the j th level, and a negative value means that it acts to decrease it. By calculating the $\Delta C_j^{(k)}(t)$ for each level, it is possible to analyze which vibrational level has the dominant contribution to the excitation process of a given level. Furthermore, by calculating the $\Delta C_j^{(k)}(t)$ for each electric field component, $E^{\text{Main}}(t)$, $E^{\text{DSP}}(t)$, we can distinguish the contributions of each pulse.

Figure 4(b) shows the occupation number of the 12th, 13th and 14th vibrational levels (lower levels than the “Missing Rung”) and the contribution from the other levels calculated by Eq. 8 for the simulation of the DSP method shown in Fig. 3(a). It can be understood that the cascade excitation of wavepacket, i.e. the VLC, is the result of the quantum interference of the positive contribution from the lower level and the slightly delayed negative contribution from the upper level. It is noteworthy that these transitions are caused by the contributions from adjacent levels, which agree with the process of quantum ladder climbing described by successive Landau-Zener transitions[16]. It is also worth mentioning that even though the electric field of the DSP is present during the transition of these levels, it does not contribute at all to the changes in occupation numbers. This indicates that the excitation processes at lower levels than the MRP region are all induced by the main pulse.

Next, we show the results for the vibrational levels of 15th, 16th, 17th and 18th (levels around the “Missing Rung”) in Fig.5. Figure5(a) shows the result with DSP shown in Fig. 3(a). and (b) shows the result without DSP shown in Fig. 3(b). Comparing the time variations of the occupation number for the 15th level, it can be seen that without the DSP (Fig.5(b)), the positive contribution of the 14th level is not sufficiently canceled out by the negative contribution from the 16th level and most of the wavepacket remains in the 15th level. Whereas with DSP (Fig.5(a)), the additional negative contribution from 17th level caused by the DSP significantly decrease the occupation number of 15th level. Seeing the contribution to the 17th level in Fig. 5, there are slight contribution from other levels without the DSP, on the other hand, there are the apparent positive contribution from 15th level with the DSP, which makes wavepackets being excited to higher levels. Such a interlevel excitation can be seen also between the 16th and 18th levels for the DSP method. These results guarantee the interpretation of MRP and the mechanism of the DSP method.

The proposed contribution values revealed that the DSP method utilizes the quantum interference effec-

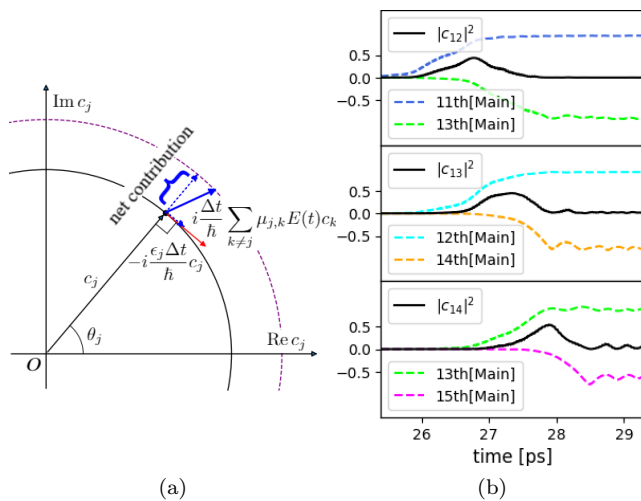


FIG. 4: (a) Schematic illustration of the Eq.7. (b) The occupation numbers $|c_j|^2(t)$ and the contributions from other levels $\Delta C_j^{(k)}(t)$ for the 12th, 13th, 14th levels.

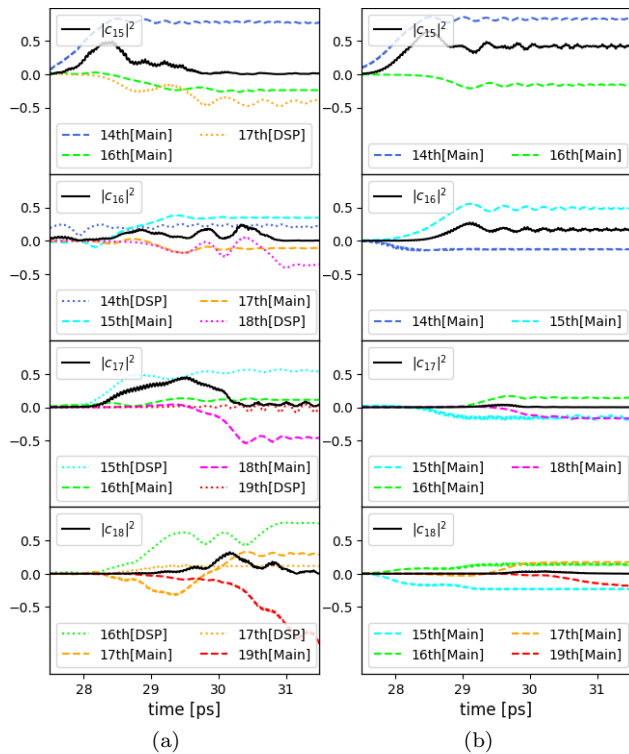


FIG. 5: The occupation numbers $|c_j|^2(t)$ and the contributions from other levels $\Delta C_j^{(k)}(t)$ for the 15th, 16th, 17th and 18th levels (a)with DSP and (b)without DSP.

tively to solve the MRP. Such quantum interference effects are one of the most important features of coherent control[29–31]. The other thing that indicates the quantum interference is the effects of the phases of electric fields. It is found that the dissociation probability changes significantly as the relative phase changes (see supplemental materials). This implies the fact that the phase of the electric field and that of the vibrational levels are coupled, and they plays the important role on the dynamics of quantum interference. Thus, the quantum interference is deeply related to the DSP method.

In summary, we simulated the photodissociations by the VLC based on the PES and dipole moment computed by highly-accurate quantum chemistry method. As a result, we found the MRP which cause the interruption of the VLC. We revealed that the MRP is caused by the disappearance of the adjacent TDM at a specific vibrational level. As a solution to this problem, we proposed the DSP method that uses additional pulses to induce $\Delta\nu = \pm 2$ transition, and verified its effect to the MRP by wavepacket dynamics simulations. It should be noted that the DSP method not only enhance the dissociation probability but also is more energy-efficient than the single pulse method. We also clarified the detail mechanisms of the VLC and DSP method: the excitation process of

the VLC is caused by the quantum interference between the positive contribution from the lower level and the negative contribution from the upper level and the DSP plays an essential role in the excitation process to higher levels. The MRP is considered to be ubiquitous problem in the VLC because it originates the parity of the vibrational wavefunction and the dipole function. The reason there are not many experimental reports of the VLC-induced molecular bond breaking might be the MRP, we believe that our findings may pave the way to the VLC-induced photodissociation and, ultimately, for versatile control of chemical reactions.

* hirotooshih@mosk.tytlabs.co.jp

- [1] Paul Brumer and Moshe Shapiro. Control of unimolecular reactions using coherent light. *Chemical physics letters*, 126(6):541–546, 1986.
- [2] David J Tannor and Stuart A Rice. Control of selectivity of chemical reaction via control of wave packet evolution. *The Journal of chemical physics*, 83(10):5013–5018, 1985.
- [3] Thomas Baumert, M Grosser, Rainer Thalweiser, and Gustav Gerber. Femtosecond time-resolved molecular multiphoton ionization: The na 2 system. *Physical review letters*, 67(27):3753, 1991.
- [4] ED Potter, JL Herek, S Pedersen, Q Liu, and AH Zewail. Femtosecond laser control of a chemical reaction. *Nature*, 355(6355):66–68, 1992.
- [5] Y Hikosaka, T Kaneyasu, M Fujimoto, H Iwayama, and M Katoh. Coherent control in the extreme ultraviolet and attosecond regime by synchrotron radiation. *Nature communications*, 10(1):1–5, 2019.
- [6] Haruka Goto, Hiroyuki Katsuki, Heide Ibrahim, Hisashi Chiba, and Kenji Ohmori. Strong-laser-induced quantum interference. *Nature Physics*, 7(5):383–385, 2011.
- [7] Szczepan Chelkowski and George N Gibson. Adiabatic climbing of vibrational ladders using raman transitions with a chirped pump laser. *Physical Review A*, 52(5):R3417, 1995.
- [8] Ikki Morichika, Kei Murata, Atsunori Sakurai, Kazuyuki Ishii, and Satoshi Ashihara. Molecular ground-state dissociation in the condensed phase employing plasmonic field enhancement of chirped mid-infrared pulses. *Nature communications*, 10(1):1–8, 2019.
- [9] DJ Maas, DI Duncan, AFG Van der Meer, WJ Van der Zande, and LD Noordam. Vibrational ladder climbing in no by ultrashort infrared laser pulses. *Chemical Physics Letters*, 270(1-2):45–49, 1997.
- [10] Gilad Marcus, Arie Zigler, and Lazar Friedland. Molecular vibrational ladder climbing using a sub-nanosecond chirped laser pulse. *EPL (Europhysics Letters)*, 74(1):43, 2006.
- [11] Mukesh Jewariya, Masaya Nagai, and Koichiro Tanaka. Ladder climbing on the anharmonic intermolecular potential in an amino acid microcrystal via an intense monocycle terahertz pulse. *Physical review letters*, 105(20):203003, 2010.
- [12] Wing-Ki Liu, Binruo Wu, and Jian-Min Yuan. Nonlinear dynamics of chirped pulse excitation and dissociation of diatomic molecules. *Physical review letters*, 75(7):1292,

- 1995.
- [13] W-K Liu, J-M Yuan, and SH Lin. Classical dynamics of multiphoton excitation and dissociation of diatomic molecules by infrared laser pulses. *Physical Review A*, 60(2):1363, 1999.
- [14] Yiwu Duan, Wing-Ki Liu, and Jian-Min Yuan. Classical dynamics of ionization, dissociation, and harmonic generation of a hydrogen molecular ion in intense laser fields: A collinear model. *Physical Review A*, 61(5):053403, 2000.
- [15] G Marcus, L Friedland, and A Zigler. From quantum ladder climbing to classical autoresonance. *Physical Review A*, 69(1):013407, 2004.
- [16] I Barth, L Friedland, O Gat, and AG Shagalov. Quantum versus classical phase-locking transition in a frequency-chirped nonlinear oscillator. *Physical Review A*, 84(1):013837, 2011.
- [17] Ido Barth and Lazar Friedland. Quantum phenomena in a chirped parametric anharmonic oscillator. *Physical review letters*, 113(4):040403, 2014.
- [18] Tsafir Armon and Lazar Friedland. Quantum versus classical dynamics in the optical centrifuge. *Physical Review A*, 96(3):033411, 2017.
- [19] Tsafir Armon and Lazar Friedland. Quantum versus classical effects in the chirped-drive discrete nonlinear schrödinger equation. *Physical Review A*, 100(2):022106, 2019.
- [20] Tsafir Armon and Lazar Friedland. Quantum versus classical chirps in a rydberg atom. *Physical Review A*, 102(5):052817, 2020.
- [21] Ido Barth, Ilya Y Dodin, and Nathaniel J Fisch. Ladder climbing and autoresonant acceleration of plasma waves. *Physical review letters*, 115(7):075001, 2015.
- [22] Yoni Shalibo, Ya'ara Rofe, Ido Barth, Lazar Friedland, Radoslaw Bialczack, John M Martinis, and Nadav Katz. Quantum and classical chirps in an anharmonic oscillator. *Physical review letters*, 108(3):037701, 2012.
- [23] JT Lin, TL Lai, DS Chuu, and Tsin-Fu Jiang. Quantum dynamics of a diatomic molecule under chirped laser pulses. *Journal of Physics B: Atomic, Molecular and Optical Physics*, 31(4):L117, 1998.
- [24] Kenji Mishima and Koichi Yamashita. A theoretical study on laser control of a molecular nonadiabatic process by ultrashort chirped laser pulses. *The Journal of chemical physics*, 109(5):1801–1809, 1998.
- [25] Thomas Witte, Thomas Hornung, Lars Windhorn, Detlev Proch, Regina de Vivie-Riedle, Marcus Motzkus, and Karl-Ludwig Kompa. Controlling molecular ground-state dissociation by optimizing vibrational ladder climbing. *The Journal of chemical physics*, 118(5):2021–2024, 2003.
- [26] David Willock. *Molecular symmetry*. John Wiley & Sons, 2009.
- [27] Péter G Szalay and Rodney J Bartlett. Multi-reference averaged quadratic coupled-cluster method: a size-extensive modification of multi-reference ci. *Chemical physics letters*, 214(5):481–488, 1993.
- [28] Nikolaus Hansen and Andreas Ostermeier. Adapting arbitrary normal mutation distributions in evolution strategies: The covariance matrix adaptation. In *Proceedings of IEEE international conference on evolutionary computation*, pages 312–317. IEEE, 1996.
- [29] Kenji Ohmori, Hiroyuki Katsuki, Hisashi Chiba, Masahiro Honda, Yusuke Hagihara, Katsutoshi Fujiwara, Yukinori Sato, and Kiyoshi Ueda. Real-time observation of phase-controlled molecular wave-packet interference. *Physical review letters*, 96(9):093002, 2006.
- [30] Hiroyuki Katsuki, Hisashi Chiba, Bertrand Girard, Christoph Meier, and Kenji Ohmori. Visualizing picometric quantum ripples of ultrafast wave-packet interference. *Science*, 311(5767):1589–1592, 2006.
- [31] Kenji Ohmori, Yukinori Sato, Evgueni E Nikitin, and Stuart A Rice. High-precision molecular wave-packet interferometry with hgar dimers. *Physical review letters*, 91(24):243003, 2003.

Supplemental Material for “Missing Rung Problem in Vibrational Ladder Climbing”

Takahiro Horiba, Soichi Shirai, and Hirotoishi Hirai*
Toyota Central Research and Development Labs., Inc.,
41-1, Yokomichi, Nagakute, Aichi 480-1192, Japan

(Dated: October 23, 2021)

I. QUANTUM CHEMISTRY COMPUTATIONS

The potential energy curves and dipole moments of the LiH and HF molecules were calculated using the multi-reference averaged quadratic coupled-cluster (MR-AQCC) method [1]. First, the complete active space self-consistent field (CASSCF) calculations [2] were carried out. Subsequently, the obtained CASSCF wavefunctions were adopted as reference functions for the MR-AQCC calculations. For LiH, the molecular orbitals derived from the Li 2s, and H 1s atomic orbitals were selected as active orbitals. The CAS was constructed by distributing two electrons over these two orbitals. In the MR-AQCC calculations, the electrons in Li 1s were additionally correlated. For HF, the molecule was placed on the z-axis. Accordingly, the H 1s and F 2pz orbitals were relevant to the formation of the H-F bond. The molecular orbitals derived from these atomic orbitals were selected as active orbitals in the CASSCF calculations; two electrons involved in these orbitals were treated as active electrons. The electrons in the orbitals originated from F 1s, F 2s, F 2px and F 2py were also correlated in the MR-AQCC calculations. The basis set used was Dunning’s aug-cc-pVQZ [3–5]. All the calculations were carried out using the GAMESS program [6, 7]. The calculated spectroscopic parameters and dipole moments were summarized in Table I. Here, the spectroscopic parameters were estimated by fitting the potential energy curve with a quadratic function. The calculated parameters were in good agreement with the corresponding experimental values [8]. The results suggest that the potential energy curves and dipole moments are reliable over the entire range. The CASSCF and MR-AQCC potential energy curves and transition dipole moments were compared in Fig. 1. The CASSCF results were quite different from the MR-AQCC results because of the lack of dynamical correlations. As a result, the “Missing Rung” in which the transition dipole moment gets closed to zero appeared at different states. The results suggest that the calculations using a high-level method is necessary to estimate the exact position of the “Missing Rung”.

TABLE I: Calculated and experimental parameters for LiH and HF. r_e are the equilibrium distances, D_0 are the dissociation energies, ω_e are the fundamental vibrational frequencies and μ are the dipole moments.

System	r_e [angst.]	D_0 [eV]	ω_e [cm ⁻¹]	μ [Debye]
LiH (calc.)	1.5710	2.496	1422.22	5.792
LiH (exp.)	1.5957	2.429	1405.65	5.882
HF (calc.)	0.9168	5.848	4103.48	1.791
HF (exp.)	0.9168	5.869	4138.32	1.826

II. DOUBLE-STEPPING TRANSITION

Here, we show the transition dipole moments (TDMs) of $\Delta\nu = \pm 2$. Figure 2(a) and (b) shows the TDMs of $\Delta\nu = \pm 1$ transitions and $\Delta\nu = \pm 2$ transitions of LiH and HF molecules. It is clearly seen that the increase and decrease of these values are just opposite, which can be accounted for by the parities of wavefunctions and the dipole moment.

* hirotoshih@mosk.tytlabs.co.jp

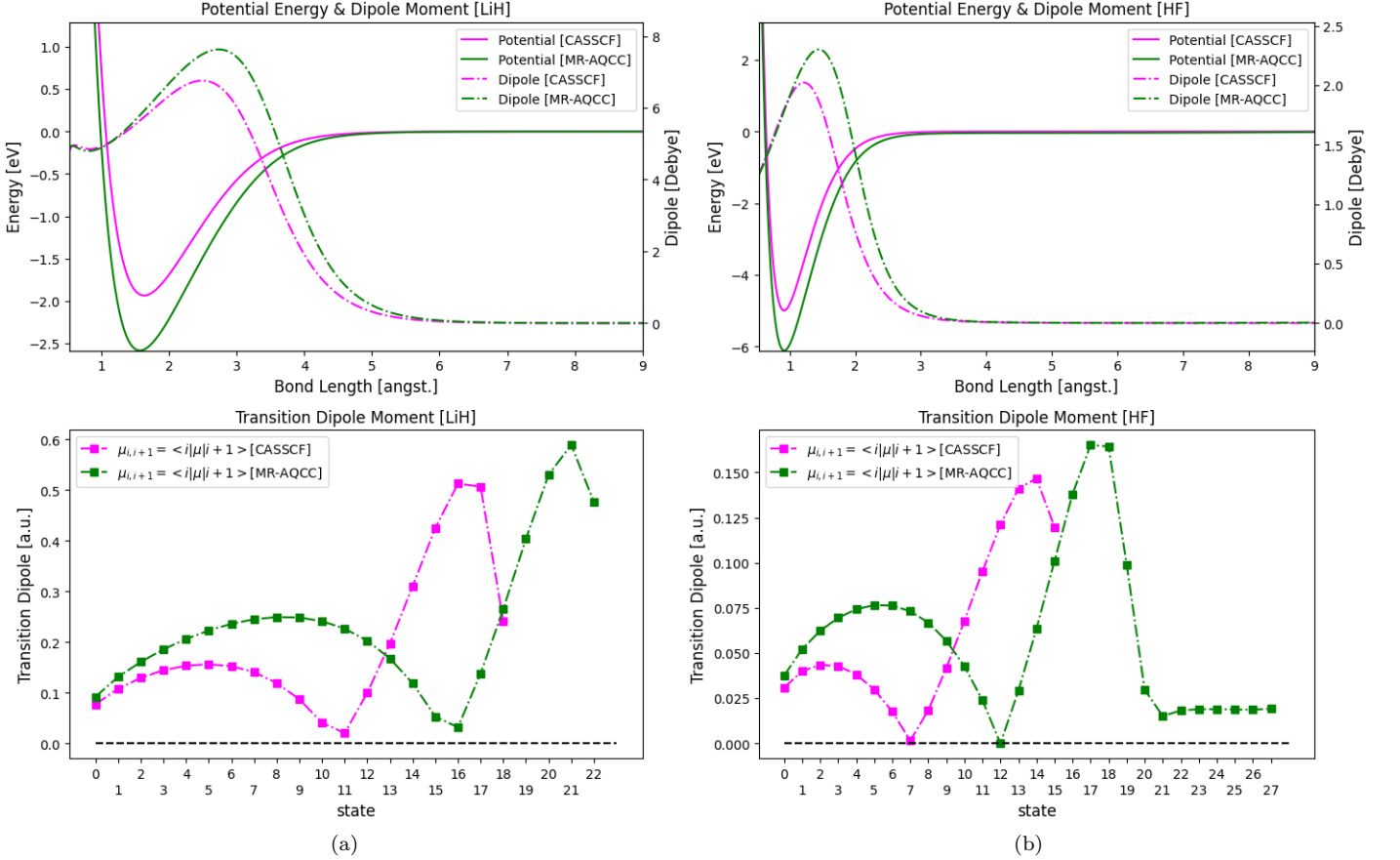


FIG. 1: Comparison between CASSCF and MR-AQCC. Upper panels: The PESs and the dipole moments for (a) LiH molecule and (b) HF molecule. Lower panels: the corresponding TDMs.

III. WAVEPACKET DYNAMICS SIMULATIONS

In non-relativity, the time evolution of quantum systems can be described by the time-dependent Schrödinger equation,

$$i\hbar \frac{\partial}{\partial t} \psi(x, t) = H(t) \psi(x, t). \quad (1)$$

The formal solution of the Schrödinger equation with the time-independent potential $V(x)$ can be written as

$$\psi(x, t) = e^{-i\frac{H(x)}{\hbar}t} \psi(x, 0), \quad (2)$$

where $U(t) = e^{-i\frac{H(x)}{\hbar}t}$ is the time evolution operator. However, we have to deal with the time-dependent Hamiltonian $H(x, t)$ that describes the system under the laser electric field $E(t)$,

$$H(x, t) = -\frac{\hbar^2}{2M} \frac{\partial^2}{\partial x^2} + V(x, t), \quad (3)$$

where $V(x, t) = V(x) - \mu(x)E(t)$. To deal the time-varying potential $V(x, t)$, we set $t = Ndt$ and express the time evolution operator as the product of N operators in time increments of dt ,

$$U(t) = \prod_{j=0}^N U_j(dt), \quad (4)$$

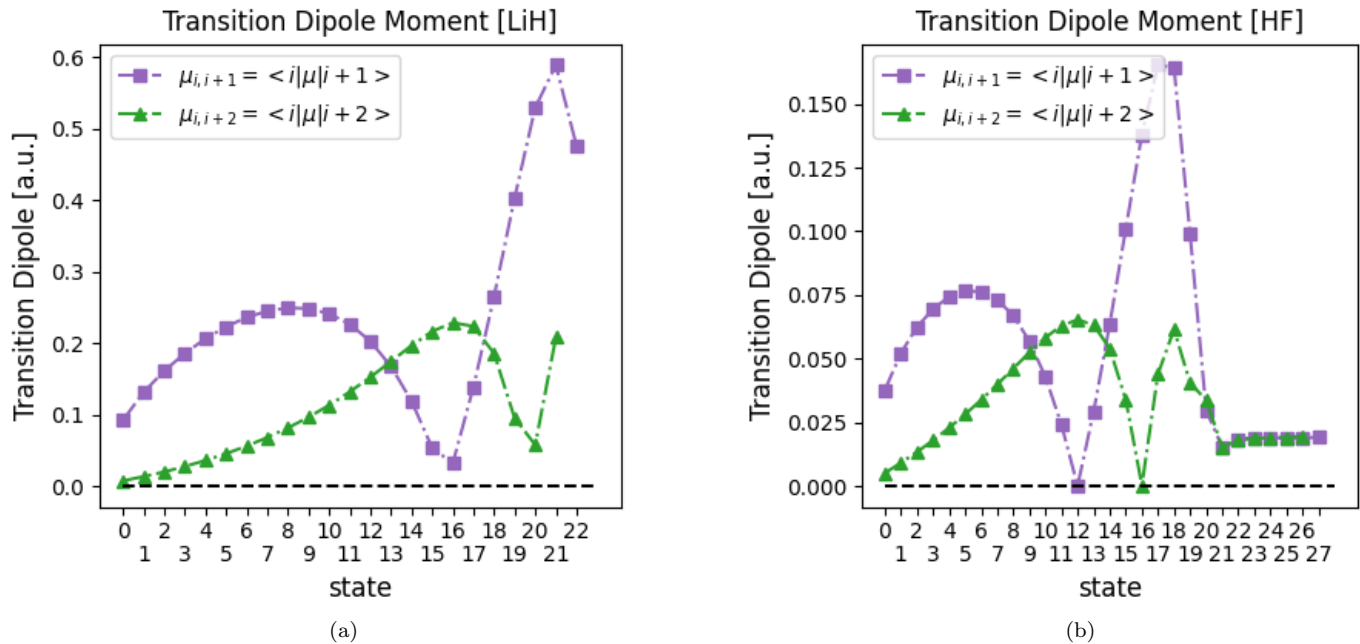


FIG. 2: TDMs of $\Delta\nu = \pm 1$ and TDMs of $\Delta\nu = \pm 2$ for (a) LiH molecule and (b) HF molecule. TDMs is calculated based on the PESs and dipole moments calculated by MR-AQCC.

where

$$U_j(dt) = e^{-i\frac{H(x,jdt)}{\hbar}dt} \quad (5)$$

As a method of operating the exponential operator on the wave function, a number of methods have been developed[9], including the methods based on Taylor expansion, Chebyshev-polynomial method etc., however, Suzuki-Trotter decomposition method[10] has been often used because of the good balance between computational cost and speed. We also use the Suzuki-Trotter decomposition method for the time-evolution computation. The second-order Suzuki-Trotter decomposition can be written as

$$U_j(dt) \sim e^{-i\frac{T}{\hbar}\frac{dt}{2}} e^{-i\frac{V(x,jdt+dt/2)}{\hbar}dt} e^{-i\frac{T}{\hbar}\frac{dt}{2}} + O(dt^3) \quad (6)$$

The error arises because T and V are non-commutative. Here, T is diagonal in wavenumber space and V is diagonal in real space, so in the second-order Suzuki-Trotter method, when applying $e^{-i\frac{T}{\hbar}\frac{dt}{2}}$, the wave function is expressed in wavenumber space using the fast Fourier transformation (FFT) and $e^{-i\frac{V(x,jdt+dt/2)}{\hbar}dt}$ is applied to the wave function which returns to real space notation by inverse FFT. When $e^{-i\frac{T}{\hbar}\frac{dt}{2}}$ is applied again, the wave function is expressed in wave number space using the FFT again. Using the above procedure, the time-evolution computation can proceed without expanding the exponential function operator. By repeating these calculations N times, the wave function at the desired time t can be obtained.

For the simulations of LiH dissociation by the chirped laser pulses, $dt = 1.0$ [a.u.] is used. The simulation time t depends on the shape of the chirped laser pulses, $t = 8\sigma$. Here σ is the standard deviation of the Gaussian envelope for the pulse laser. We take the evenly spaced isotropic grid of 2^{10} elements for x . As the range of x , we take $x = 1.5 - 15.0$ [bohr].

A. Dissociation probability

Here, we describe how to calculate the dissociation probability. The wavefunctions that reach the right edge of the grid represent the state of bond-dissociation. Therefore, the probability densities $|\psi(x_{right-edge})|^2$ represents the dissociation probability. it is convenient to use the probability density flux,

$$J(x,t) = \frac{\hbar}{2iM}(\psi^*(x,t)\nabla\psi(x,t) - (\nabla\psi(x,t))^*\psi(x,t)) = Re(\psi(x,t)^*\frac{\hbar}{iM}\nabla\psi(x,t)). \quad (7)$$

$\frac{\hbar}{iM}\nabla\psi(x,t)$ can be transformed as the following,

$$\frac{\hbar}{iM}\nabla\psi(x,t) = \hat{p}\psi(x,t)/M = IFFT(k\psi(p,t))/M, \quad (8)$$

where *IFFT* means inverse FFT. Thereby we can compute $\frac{\hbar}{iM}\nabla\psi(x,t)$ fast because we have the wavefunction in wave number space $\psi(p,t)$ to use the Suzuki-Trotter decomposition method for the time-evolution computation. The time integral of the probability density flux at the right edge of the grid after sufficiently long simulation time gives the dissociation probability in this case.

$$P_{dissociation} = \int_0^t J(x_{right-edge}, t') dt' \quad (9)$$

B. complex absorbing potential

An absorption potential with a negative pure imaginary value was set to prevent the wavefunction from reaching the grid boundary. Here, we used the complex absorption potential of the 4th order function,

$$V_{absorbing}(x) = -i\alpha x^4 \quad (10)$$

where $\alpha = 1.0$ is used in this study. The norm of the wave function reaching the region where this function has a significant value decays. This prevents reflections at the edge and the unnecessary interference caused by them. It was placed just after the flux calculation point.

IV. THE RANGE OF LASER PARAMETERS

Since the MRP is a quantum problem that appears when vibrational levels can be regarded as discrete, we have to choose laser parameters (E_0 : the maximum electric field intensity, α : the spreading parameter of the Gaussian) that reproduce the excitation process where the quantum mechanics is dominant. Here, we explain a rough estimation of the laser parameter range where quantum ladder climbing occurs, using the parameters proposed by Friedland et al. to distinguish between quantum ladder climbing and classical autoresonance[11].

The excitation process is characterized by three time scales as follows, $T_R = \sqrt{2m\hbar\omega_0}/\epsilon$, $T_S = 1/\sqrt{\alpha}$, $T_{NL} = 2\omega_0\beta/\alpha$ where m is the reduced mass, ω_0 is the eigenfrequency, β is the anharmonicity of system. ϵ is the manitude of external field, and α is the chirp rate.

To obtain the values of ω_0 and β of LiH, the excitation frequency is fitted with the following equation.

$$\omega_{n,n+1} = \omega_0[1 - 2\beta(n+1)] \quad (11)$$

The reults of fitting is $\omega_0 = 0.0068[a.u.]$, $\beta = 0.0176$.

ϵ corresponds to the product of the electric field and the linear dipole moment. Although the dipole moment of LiH is nonlinear, that in the range of 2-5.5 [Bohr], is linearly approximated to be $\mu(x) = 0.354x + 1.086$. The effective external field magnitude ϵ^{eff} is estimated as $\epsilon^{\text{eff}} = 0.354E_0$. The chirp rate is taken as the value when $\gamma_1 = \gamma_2 = 0.5$ ($= \omega_{0 \rightarrow 1}/4\sigma$).

Based on these values, T_R, T_S, T_{NL} is calculated and, the parameters that distinguish quantum from classical P_1, P_2 are expressed as follows,

$$P_1 = \frac{T_S}{T_R}, \quad (12)$$

$$P_2 = \frac{T_{NL}}{T_S}. \quad (13)$$

The conditions under which phase-locked ladder climbing occurs are as follows,

$$P_2 > P_1 + 1, \quad (14)$$

$$P_1 > 0.79. \quad (15)$$

Figure 3 shows the calculated value of $P_2 - (P_1 + 1)$ for the parameter range of $E_0 = 10^{-1} - 10^2$, $\alpha = 10^{-9} - 10^{-6}$. The parameter range that satisfy the conditions Eq. 15 is colored in red. From Fig. 3, ladder climbing is considered

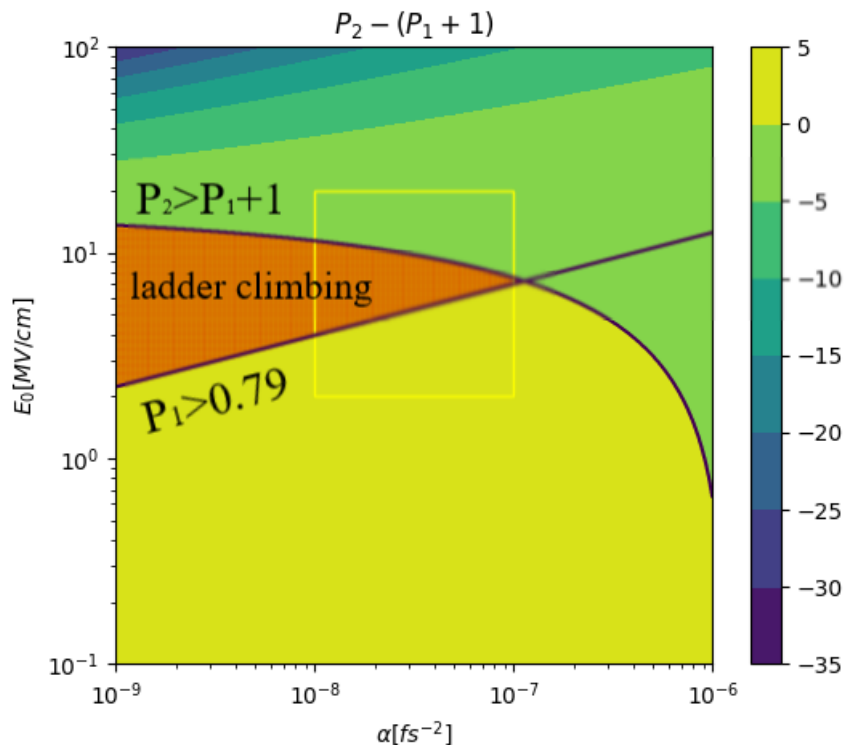


FIG. 3: The characterization parameter $P_2 - (P_1 + 1)$ calculated in the range of $E_0 = 10^{-1} - 10^2$, $\alpha = 10^{-9} - 10^{-6}$. The parameter range corresponding the quantum ladder climbing is colored red. Yellow boxed area represents the parameter ranges we chose.

to occur in the parameter range of $E_0 = 2.0 - 20$ [MV/cm], $\alpha < 10^{-7}$ [fs $^{-2}$]. As for α , it is not possible to make it arbitrarily small due to vibrational relaxation time. We refer to the vibrational lifetime of the CO stretching measured by Kemlin et al.[12] and assume a time scale for vibrational relaxation to be a few tens of ps, which corresponds to the parameter range of $\alpha = 10^{-8} - 10^{-7}$ [fs $^{-2}$]. Based on the above estimation, we set the parameter range as $E_0 = 2.0 - 20$ [MV/cm], $\alpha = 10^{-8} - 10^{-7}$ [fs $^{-2}$] (yellow boxed area in the Fig. 3). Note that more detailed discussion is required for actual system to obtain more accurate characterization.

V. OPTIMIZATION OF THE CHIRPED LASER PULSE PARAMETERS

Here, we describe the details of the optimization methods of chirped laser parameters. we adopted following linear chirped frequency as time-dependent frequency $\omega(t)$ of laser pulse.

$$\omega(t) = \omega_0 \left\{ -(\gamma_1 + \gamma_2) \cdot \frac{t - t_0}{4\sigma} + 1 + \frac{\gamma_1 - \gamma_2}{2} \right\}, \quad (16)$$

Equation 16 is parametrized by the two dimensionless parameters γ_1 and γ_2 . These chirp parameters significantly affects the excitation process of vibrational ladder climbing(VLC). In order to achieve more effective excitation, we optimized these parameters using a combination of machine learning and wavepacket dynamics simulation. That is, machine learning updates the parameters based on the evaluated values of the parameters obtained by wavepacket dynamics simulation.

In the case of single pulse, the parameters to be optimized are two parameters (γ_1 and γ_2), whose value ranges are restricted to $[0, 1]$ so as to represent the downchirp. This parameter space is divided into a 100×100 grids (i.e. 0.01 steps), and the optimal parameter is searched from these grid points by optimization method.

The chirp parameters are optimized for each of 400 different pulses, thus fast and efficient optimization method is required. In addition, since the effects of parameters on excitation process are not able to evaluate analytically, this system is regarded as black-box. As a fast optimization method for such black-box optimization, we employed Bayesian optimization. Bayesian optimization enables efficient exploration and optimization in parameter space leveraging

predictive models such as Gaussian process regression, which is a powerful method for black-box optimization[13]. We have used GPy[14], an open source library in python, as an implementation of Bayesian optimization. In Bayesian optimization, we adopted Gaussian process regression with the RBF(Radial Basis Function) kernel as the predictive model for the parameter space, and employed the UCB(Upper Confidential Bound) as the acquisition function. The iteration number for updating parameters was set to 50.

The objective function was set to be the sum of the excited and dissociated wavepacket. Although we aim to find parameters for efficient photodissociation, for some pulse parameters whose energy is not enough to cause dissociation, objective function with only the amount of dissociation will result in insufficient optimization. Therefore, by including an amount of excited wavepacket in addition to that of dissociated wavepacket in the objective function, it is possible to obtain optimized parameters that realize efficient excitation. The amount of dissociated wavepacket is evaluated by integrating the absorbed wavepacket described in the previous section. The degree of excitation is evaluated by the expected value of occupied states $|\phi_i\rangle$ as follows,

$$P_{\text{excited}} = \sum_{i=0}^{n_{\text{dissoc}}} \left(\frac{i}{n_{\text{dissoc}}} \right) |\langle \phi_i | \psi(x, t) \rangle|^2, \quad (17)$$

where n_{dissoc} is the highest level in the bound state, and $n_{\text{dissoc}} = 23$ in the case of LiH. The expected value of the level is normalized by n_{dissoc} in order to balance the amount of dissociation whose value range is $[0, 1]$. Based on above settings, the optimization of chirp parameters was performed in the single pulse case.

In the case of DSP method, parameters to be optimized are five parameters, that are chirp parameters of main pulse and DSP ($\gamma_1^{\text{Main}}, \gamma_2^{\text{Main}}, \gamma_1^{\text{DSP}}, \gamma_2^{\text{DSP}}$), and the delay time between main pulse and DSP ($\Delta t_0 = t_0^{\text{DSP}} - t_0^{\text{Main}}$).

Since the computational cost of Bayesian optimization increases in proportion to the cube of the number of variables[15], it is difficult to handle five variables in Bayesian optimization. Thus, CMA-ES[16] was used for optimization. CMA-ES is a method that adaptively updates and optimizes the covariance matrix of the multivariate normal distribution that generates candidate solutions based on the evaluation values of the candidates. It is known that CMA-ES is a robust method that can be optimized even in noisy high-dimensional parameter spaces[17, 18].

In the optimization using CMA-ES, the number of generations was set to 150, and the number of individuals to 16 for each generation. The objective function was set to be only the amount of dissociated wavepacket because a certain amount of dissociation can be expected by adding DSP. The initial values of $\gamma_1^{\text{Main}}, \gamma_2^{\text{Main}}$ is inherited from the optimal parameters for a single pulse case. The value range of parameters is not restricted, allowing the parameters to be negative values. Negative parameter values give the possibility of upchirping or the DSP reaching ahead of the main pulse.

VI. ESTIMATION OF ENERGY EFFICIENCY

To determine the energy efficiency of photodissociation by VLC, the energy of the laser pulse and the amount of dissociated molecules is required to be estimated. Here, we show the rough estimation of those values. First, we explain how to estimate the energy of a pulse. The electric field of Gaussian pulsed laser $E(t)$ is determined by the maximum electric field intensity E_0 , the spreading parameter of the Gaussian α , as follows,

$$E(t) = E_0 \exp^{-\alpha(t-t_0)^2} \cos \omega(t)(t - t_0), \quad (18)$$

The irradiance $I[\text{W}/\text{cm}^2]$ of a pulsed laser is expressed with the maximum electric field intensity $E_0[\text{V}/\text{cm}]$ as follows[19]

$$I = \frac{c\epsilon_0 n}{2} E_0^2, \quad (19)$$

where c, ϵ_0 and n are the speed of light, dielectric constant, and refractive index of the vacuum, respectively. The energy of a pulse $e[\text{J}]$ is expressed by the irradiance $I[\text{W}/\text{cm}^2]$, pulse width $T[\text{s}]$, and cross section of pulse $S[\text{cm}^2]$ as follows,

$$e = STI \simeq 0.002 \cdot \frac{E_0^2 S}{\sqrt{\alpha}}, \quad (20)$$

where pulse width $T[\text{s}]$ is defined as the full width at half maximum of the Gaussian pulse, $T = 2\sqrt{2 \log 2} \sigma \simeq 2.23/\sqrt{2\alpha}$. In the case of single pulse, the total energy to be required to cause VLC is calculated by Eq.20. In the case of DSP method, the two pulses, the main pulse and the DSP, are required for the VLC. We assume that the optical system

for the implementation of the DSP method is like that used in pump-probe spectroscopy with single light source. Assuming that there is no energy loss in such an optical system, the total energy required for VLC become the sum of the main pulse and DSP energy. Since this is a very rough estimate, the more energy is considered to be required for DSP method in practice.

Next, we explain the calculation method for the amount of dissociated molecular. The amount of molecules $N_{\text{all}}[\text{mol}]$, present in the region of the pulse cross section $S[\text{cm}^2]$, can be written as $N_{\text{all}} = \rho S$, where $\rho[\text{mol}/\text{cm}^2]$ is the areal density of the molecules. Assuming that the laser pulse causes dissociation with a dissociation probability d , the amount of dissociated molecules $N_{\text{dissoc}}[\text{mol}]$ is given by,

$$N_{\text{dissoc}} = N_{\text{all}}d = \rho Sd. \quad (21)$$

For simplicity, we assume that $\rho = 1[\text{mol}/\text{cm}^2]$.

From Eqs. 20 and 21, the energy efficiency $P[\text{mol}/\text{J}]$ of photodissociation by VLC can be estimated as follows,

$$P = \frac{N_{\text{dissoc}}}{e} \simeq 478 \cdot \frac{d\sqrt{\alpha}}{E_0^2}. \quad (22)$$

Based on the above formulation, we estimated the energy efficiency for the results of single-pulse case and the DSP method, respectively.

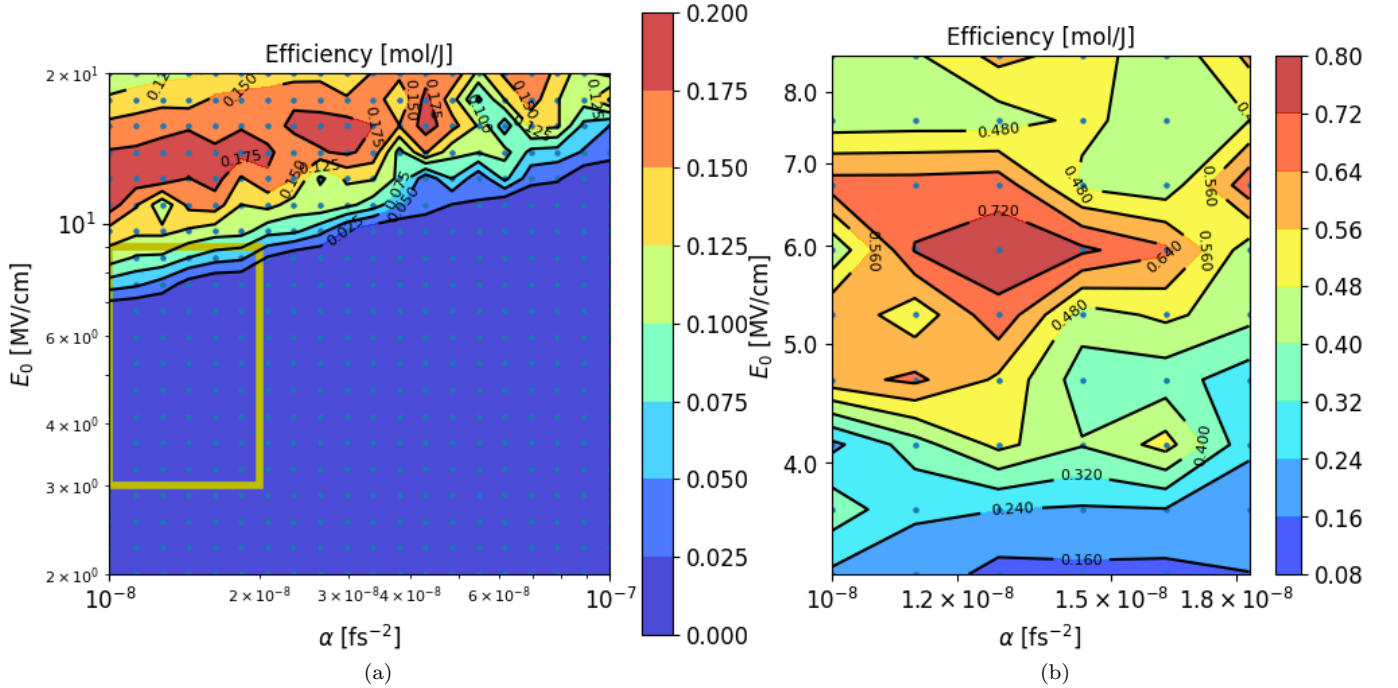


FIG. 4: Calculated energy efficiencies for (a)single pulse and (b)DSP method

Figure 4 shows the calculated energy efficiency of each case. It can be seen that the DSP method shows higher energy efficiency than the single pulse case. The maximum energy efficiency for a single pulse is 0.193 [mol/J], while that for the DSP method is 0.763 [mol/J], which is about four folds higher. This result shows the superiority of the DSP method with respect to energy efficiency.

VII. THE EFFECT OF RELATIVE PHASE

In the optimization of the parameters of DSP method, the relative phase between the electric field of the main pulse and that of the DSP was fixed at zero. This is because the relative phase changes significantly with changes in the parameters such as chirp parameters, making it difficult to optimize it simultaneously with those parameters. However, the effect of relative phase can not be negligible, since it affects the time evolution of probability amplitudes of vibrational levels. In this section, we discuss the effect of the relative phase between the main pulse and DSP on the photodissociation by DSP method.

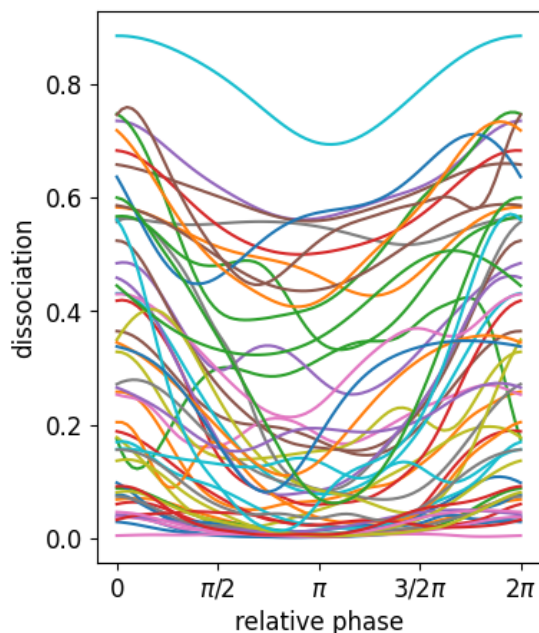


FIG. 5: The relationship between the dissociation probability and relative phases.

For the 54 pulses considered in DSP method with optimized parameters at the relative phase of zero, we performed wavepacket dynamics simulation by varying the relative phases from 0 to 2π ,

Figure 5 shows the relationship between dissociation probability and relative phase. From Fig. 5, it is revealed that the relative phase has a significant effect on the dissociation probability. The change in relative phase affects the phase of the probability amplitude of the vibrational levels and changes the appearance of the interference between them, which leads to change the dissociation probability shown in Fig.5. Therefore, this result can be attributed to the quantum interference effect between the vibration levels.

In addition, it is noteworthy that the relationship between the dissociation probability and the relative phase is approximately cosine functional. Since the optimization was performed with the relative phase fixed at zero, the optimized parameters were considered to have been chosen to maximize the dissociation probability at phase of zero. The fact that the dissociation probability becomes minimum at relative phase of π , that is the antiphase to the case of zero, is a characteristic result in interference phenomena. Since the excitation process results from the complex interference between many vibrational levels, it is not obvious that such a cosine functional relationship appears between dissociation probability and relative phase. The complete interpretation of this results will require more detailed discussion.

-
- [1] Péter G Szalay and Rodney J Bartlett. Multi-reference averaged quadratic coupled-cluster method: a size-extensive modification of multi-reference ci. *Chemical physics letters*, 214(5):481–488, 1993.
 - [2] Björn O Roos, Peter R Taylor, and Per EM Sigbahn. A complete active space scf method (casscf) using a density matrix formulated super-ci approach. *Chemical Physics*, 48(2):157–173, 1980.
 - [3] Thom H Dunning Jr. Gaussian basis sets for use in correlated molecular calculations. i. the atoms boron through neon and hydrogen. *The Journal of chemical physics*, 90(2):1007–1023, 1989.
 - [4] Rick A Kendall, Thom H Dunning Jr, and Robert J Harrison. Electron affinities of the first-row atoms revisited. systematic basis sets and wave functions. *The Journal of chemical physics*, 96(9):6796–6806, 1992.
 - [5] Brian P Prascher, David E Woon, Kirk A Peterson, Thom H Dunning, and Angela K Wilson. Gaussian basis sets for use in correlated molecular calculations. vii. valence, core-valence, and scalar relativistic basis sets for li, be, na, and mg. *Theoretical Chemistry Accounts*, 128(1):69–82, 2011.
 - [6] Michael W Schmidt, Kim K Baldridge, Jerry A Boatz, Steven T Elbert, Mark S Gordon, Jan H Jensen, Shiro Koseki, Nikita Matsunaga, Kiet A Nguyen, Shujun Su, et al. General atomic and molecular electronic structure system. *Journal of computational chemistry*, 14(11):1347–1363, 1993.
 - [7] Mark S Gordon and Michael W Schmidt. Advances in electronic structure theory: Gamess a decade later. In *Theory and applications of computational chemistry*, pages 1167–1189. Elsevier, 2005.

- [8] Klaus-Peter Huber. Constants of diatomic molecules. *Molecular spectra and molecular structure*, 1979.
- [9] W Van Dijk and FM Toyama. Accurate numerical solutions of the time-dependent schrödinger equation. *Physical Review E*, 75(3):036707, 2007.
- [10] Thomas Barthel and Yikang Zhang. Optimized lie–trotter–suzuki decompositions for two and three non-commuting terms. *Annals of Physics*, 418:168165, 2020.
- [11] I Barth, L Friedland, O Gat, and AG Shagalov. Quantum versus classical phase-locking transition in a frequency-chirped nonlinear oscillator. *Physical Review A*, 84(1):013837, 2011.
- [12] Vincent Kemlin, Adeline Bonvalet, Louis Daniault, and Manuel Joffre. Transient two-dimensional infrared spectroscopy in a vibrational ladder. *The journal of physical chemistry letters*, 7(17):3377–3382, 2016.
- [13] Jasper Snoek, Hugo Larochelle, and Ryan P Adams. Practical bayesian optimization of machine learning algorithms. *Advances in neural information processing systems*, 25, 2012.
- [14] GPy. GPy: A gaussian process framework in python. <http://github.com/SheffieldML/GPy>, since 2012.
- [15] Neil Lawrence, Matthias Seeger, and Ralf Herbrich. Fast sparse gaussian process methods: The informative vector machine. In *Proceedings of the 16th annual conference on neural information processing systems*, number CONF, pages 609–616, 2003.
- [16] Nikolaus Hansen and Andreas Ostermeier. Adapting arbitrary normal mutation distributions in evolution strategies: The covariance matrix adaptation. In *Proceedings of IEEE international conference on evolutionary computation*, pages 312–317. IEEE, 1996.
- [17] Nikolaus Hansen. The cma evolution strategy: A tutorial. *arXiv preprint arXiv:1604.00772*, 2016.
- [18] Ilya Loshchilov, Marc Schoenauer, and Michèle Sebag. Bi-population cma-es algorithms with surrogate models and line searches. In *Proceedings of the 15th annual conference companion on Genetic and evolutionary computation*, pages 1177–1184, 2013.
- [19] David B Foote, Y Lin, Liang-Wen Pi, JM Ngoko Djiokap, Anthony F Starace, and WT Hill III. Ionization enhancement and suppression by phase-locked ultrafast pulse pairs. *Physical Review A*, 96(2):023425, 2017.